Science World Journal Vol. 20(No 4) 2025 https://dx.doi.org/10.4314/swj.v20i4.4
www.scienceworldjournal.org
ISSN: 1597-6343 (Online), ISSN: 2756-391X (Print)
Published by Faculty of Science, Kaduna State University

A MODIFIED REACTION–DIFFUSION MODEL OF SELF-ORGANIZED STRUCTURES OF RADIATION DEFECTS

*S.O. Akintunde, D.O. Kehinde

Department of Basic Sciences, Babcock University, Ilishan-Remo, Ogun State, Nigeria

*Corresponding Author Email Address: akintundes@babcock.edu.ng

ABSTRACT
Radiation damage in metals produces complex spatial and temporal patterns of point defects. These defects strongly influence swelling, creep, and structural reliability in nuclear environments. Classical rate-theory models describe only the average defect concentration. They cannot explain the formation of spatially organized microstructures. Earlier continuum models, such as Selyshchev's reaction–diffusion model, introduced elastic interactions to describe defect ordering. However, those models were deterministic and relied on oversimplified physical assumptions. In this study, we present a modified reaction–diffusion model that overcomes these limitations. The model introduces three major extensions. First, it includes a spatially resolved temperature field that accounts for heat diffusion and recombination heating. Second, it incorporates stochastic defect generation using multiplicative Ornstein–Uhlenbeck noise to represent irradiation randomness. Third, it introduces nonlocal elastic interactions described by a tunable Fourier kernel that controls the interaction range. Numerical simulations in this study show a noise-induced transition from uniform defect accumulation to persistent periodic structures with alternating defect-rich and defect-poor regions. Fourier analysis results identify a dominant wavelength that scales linearly with the elastic interaction range. Simulations for iron (Fe), nickel (Ni), and tungsten (W) reproduce experimentally observed defect spacings and clustering behaviour. Parameter sweep results yield a state diagram that distinguishes uniform, patterned, and noise-dominated regimes. The results show that stochastic fluctuations play a constructive role in defect self-organization. Elastic interactions determine the spatial scale of the resulting structures. The proposed framework provides a predictive link between microscopic irradiation kinetics and experimentally observed defect patterns in metals.

Keywords: Radiation defects, Self-organization, Reaction–diffusion model, Elastic interactions, Noise-induced pattern formation, Defect dynamics

INTRODUCTION
Radiation damage in crystalline solids remains a major challenge in nuclear materials science. When a crystal is exposed to energetic particles such as neutrons, ions, or electrons, a large number of atomic displacements are produced (Akintunde and Selyshchev, 2016; [a]Akintunde *et al*., 2025; [b]Akintunde *et al*., 2025). These displacement events create vacancies, interstitials, and defect clusters. At high doses, the accumulation of such defects causes significant microstructural changes that degrade the mechanical and thermal properties of materials.

Irradiation-induced phenomena such as swelling, creep, hardening, and embrittlement severely limit the performance of structural components in nuclear reactors and fusion devices (Mansur and Bloom, 1982; Garner, 2020; Fukuya, 2013; Griffiths, 2021; Zinkle and Snead, 2014; Dubey and El-Azab, 2013). Understanding how defects evolve under irradiation is therefore both scientifically and technologically important.

A notable feature of radiation damage is that defects often self-organize into spatially ordered patterns rather than remaining uniformly distributed. Transmission electron microscopy has revealed void lattices, dislocation loop arrays, and periodic defect-rich domains in various metals and alloys (Vainshtein *et al*., 1997; Ma *et al*., 2022; Mason *et al*., 2014; Ustrzycka *et al*., 2024; Snopiński, 2023; Li *et al*., 2019). These ordered microstructures significantly affect macroscopic properties. For instance, void lattices can stabilize defect configurations and reduce swelling (Wang *et al*., 2016; Rouxel *et al*., 2016), while dislocation patterns can alter creep response by serving as defect sinks (Patra and McDowell, 2012; Griffiths, 2023). The spontaneous emergence of such patterns shows that defect evolution is a far-from-equilibrium dynamical process.

Several theoretical frameworks have been proposed to describe radiation defect kinetics. Classical rate-theory models treat the evolution of average defect concentrations through coupled differential equations. These equations account for generation, recombination, clustering, and annihilation at sinks (Rottler *et al*., 2005; Doan and Martin, 2003; Ahmed and El-Azab, 2018; Martinez *et al*., 2020; Kohnert and Wirth, 2015; Rokkam *et al*., 2009; Gao *et al*., 2018). While these models predict mean defect densities effectively, they are spatially homogeneous and cannot describe self-organized structures. Extensions that include diffusion provide limited improvement (Hu *et al*., 2021; Yoshiie, 2025), but most remain deterministic and ignore stochastic fluctuations in irradiation.

A major step forward was introduced by Selyshchev (2003), who developed a reaction–diffusion model incorporating elastic interactions between defects. This framework includes diffusion, recombination, and long-range elastic forces, which allow instabilities that lead to periodic defect ordering. The model successfully explains void lattice formation and related structures, demonstrating that elasticity can destabilize uniform defect distributions.

Despite its pioneering contribution, Selyshchev's model exhibits several limitations.
First, temperature was treated as a uniform scalar, neglecting local heating from recombination or displacement cascades. Second, the deterministic formulation ignored stochastic bursts of defect generation, which are essential for initiating self-organization (Yao

et al., 2025; Zhang *et al*., 2023). Third, the representation of elastic interactions did not permit systematic control of the interaction range. This limitation reduced the model's ability to predict scaling relations between interaction length and defect wavelength.

To overcome these limitations, a modified reaction–diffusion model is developed in the present work. The new formulation introduces three key improvements:
(1) A spatially resolved temperature field is implemented through a heat balance equation. This equation includes diffusion, cooling, and recombination heating, enabling coupling between defect dynamics and local temperature variations.
(2) Stochastic defect generation is modeled using multiplicative Ornstein–Uhlenbeck noise. This approach describes the burst-like nature of irradiation and allows analysis of noise-induced transitions.
(3) A tunable Fourier-space kernel represents nonlocal elastic interactions. This representation enables systematic examination of how the interaction range determines the characteristic defect spacing.

Numerical simulations based on this formulation indicate that stochastic fluctuations promote defect self-organization. Elastic interactions, on the other hand, govern the characteristic wavelength of the resulting structures. This establishes a predictive link between microscopic defect dynamics and mesoscale pattern formation in irradiated metals.

MATERIALS AND METHODS

Materials/Theoretical Model

The problem under consideration is the self-organization of irradiation-induced point defects. These defects appear in a crystalline solid exposed to continuous particle flux.
Irradiation produces a stochastic distribution of vacancies and interstitials. These defects subsequently undergo diffusion, recombination, and interaction with the crystal's elastic field. Under certain conditions, these processes lead to the emergence of ordered microstructures. The present model aims to provide a minimal continuum description. It incorporates deterministic defect kinetics. It also includes the essential stochastic and elastic mechanisms that govern spatial ordering.

The evolution of the defect density field $n(x, t)$ [m^{-3}] in one spatial dimension is described by the following reaction–diffusion equation:

$$\frac{\partial n(x,t)}{\partial t} = D\nabla^2 n - \beta(T)n - \alpha n^2 + K(x,t) - V_0 \int G(x - x')n(x',t)\,dx' \quad (1)$$

Here n [m^{-3}] is the local defect density, D [$m^2.s^{-1}$] is the diffusion coefficient,

$\beta(T)$ [s^{-1}] is the temperature-dependent recombination rate with interstitials, α is the nonlinear clustering or sink absorption coefficient, $K(x, t)$ [$m^{-3}.s^{-1}$] is the stochastic defect generation rate due to irradiation, V_0 is the elastic interaction strength, and $G(x - x')$ is the elastic kernel that describes the influence of defects at position x' on those at position x. The first term on the right-hand side represents diffusion of defects, the second and third terms account for recombination and clustering, the fourth term is the source of defects from irradiation, and the last term introduces long-range elastic coupling.

The temperature field $T(x, t)$ [K] evolves according to a local heat balance equation:

$$\rho c_p \frac{\partial T(x,t)}{\partial t} = k\nabla^2 T - h(T - T_e) + Q(x,t) + \theta\beta(T)n \quad (2)$$

In this expression, ρc_p [$J.kg^{-1}.m^{-3}$] is the volumetric heat capacity, k [$W.m^{-1}.K^{-1}$] is the thermal conductivity, h [$W.m^{-2}.K^{-1}$] is the heat transfer coefficient to the surrounding medium at temperature T_e [K], $Q(x, t)$ [$K.s^{-1}$] is the external heating rate, and $\theta\beta(T)n$ [$K.s^{-1}.m^{-3}$]represents recombination heating due to annihilation of defects. This formulation introduces spatial temperature variations and feedback from defect kinetics to the thermal field.

The irradiation-induced source terms are stochastic in nature. They are modeled as:

$$K(x,t) = K_0\big(1 + \varepsilon(x,t)\big), \quad (3)$$
$$Q(x,t) = Q_0\big(1 + \epsilon(x,t)\big)$$

where K_0 [$m^{-3}.s^{-1}$] and Q_0 [$K.s^{-1}$] are the mean generation and heating rates, while $\varepsilon(x,t)$ and $\epsilon(x,t)$ are Ornstein–Uhlenbeck (O-U) noise processes. Unlike white noise, O-U noise has a finite correlation time. It describes the burst-like, memory-dependent nature of displacement cascades. It also provides a physically realistic way to study how fluctuations drive pattern formation.

An elastic interaction energy functional is introduced to model the long-range elastic coupling between point defects. Its variational derivative produces the nonlocal convolution term in Eq. (4).

The elastic interaction energy [J] is taken as the quadratic functional

$$E_{el} = \frac{V_0}{2}\iint n(x)\,G(x - x')n(x')dxdx', \quad (4)$$

The functional derivative of E_{el} with respect to $n(x)$ is

$$\frac{\delta E_{el}}{\delta n(x)} = V_0 \int G(x - x')n(x')dx'. \quad (5)$$

The elastic contribution in the defect evolution equation is introduced as the negative gradient of the elastic energy (sign convention chosen so that positive V_0 corresponds to an energetically penalizing interaction).
This yields the nonlocal term appearing in Eq. (4):

$$-\frac{\delta E_{el}}{\delta n(x)} = -V_0 \int G(x - x')n(x')dx'. \quad (6)$$

A convenient and physically transparent choice for G is the Green's function of the screened Helmholtz (Yukawa) operator,

$$(1 - l^2\nabla^2)G(x) = \delta(x), \quad (7)$$

where l the interaction (screening) length. Fourier transformation of Eq. (7) gives

$$\hat{G}(k) = \frac{1}{1+(kl)^2}, \quad (8)$$

Science World Journal Vol. 20(No 4) 2025 https://dx.doi.org/10.4314/swj.v20i4.4
www.scienceworldjournal.org
ISSN: 1597-6343 (Online), ISSN: 2756-391X (Print)
Published by Faculty of Science, Kaduna State University

Equation (8) corresponds to exponential screening in real space. In one spatial dimension, the inverse transform yields the closed form

$$G(x) = \frac{1}{2l} e^{-\frac{|x|}{l}} \text{(one-dimension)}, \quad (9)$$

so that the elastic coupling decays exponentially on the length scale l [m]. In higher dimensions, the kernel retains an exponentially screened (Yukawa) character: in two dimensions $G(r) \alpha k_0\left(\frac{r}{l}\right)$ (modified Bessel function) and in three dimensions $G(r) \alpha \frac{e^{\frac{-r}{l}}}{r}$ (Yukawa form), where $r = \|x - x'\|$.

Physically, l represents the distance over which elastic perturbations exert a significant influence. It incorporates screening effects that may arise from microstructural sinks such as dislocations and grain boundaries. It also accounts for elastic damping and other relaxation mechanisms.
The parameter V_0 controls the overall strength of the elastic coupling and is related to the elastic constants and defect relaxation volumes.
In practice, V_0 and l can be estimated from linear-elastic calculations or derived from atomistic energetics.

Equations (1)–(3) and (8) together constitute the physical model. They are solved numerically in a periodic domain. A spectral method is used for the diffusion and nonlocal terms. Stochastic contributions are integrated using the Euler–Maruyama method. The solutions are analyzed to determine the conditions for self-organization. They are also used to identify the characteristic wavelengths of emerging patterns. Finally, the analysis establishes how noise amplitude and interaction range control the spatial scale of defect structures.

Numerical Methods

The coupled system of equations (1) – (3) and (8) cannot be solved analytically. This is due to the presence of nonlinear and stochastic terms. For this reason, numerical integration is employed. It is used to investigate the spatio-temporal evolution of the defect density $n(x, t)$ and the temperature field $T(x, t)$. The method is designed to ensure stability of the diffusive and nonlocal contributions. It also properly accounts for the stochastic forcing.

The calculations are performed in a one-dimensional periodic domain of length L. The domain is divided into N equidistant grid points with spacing $\Delta x = L/N$. Periodic boundary conditions are imposed on both the defect density and the temperature field. These conditions reflect the translational invariance of an extended crystalline medium under irradiation.

Time integration is carried out using a mixed explicit–implicit strategy. The linear diffusive term and the nonlocal elastic interaction are evaluated in Fourier space. A semi-implicit spectral scheme is applied, which guarantees numerical stability at moderate time steps. The nonlinear terms, which describe recombination and clustering, are treated explicitly at each step. Recombination heating in the temperature equation is also treated explicitly.

The stochastic source terms in $K(x, t)$ and $Q(x, t)$ are integrated according to the Euler–Maruyama method. This method is well-suited for Ornstein–Uhlenbeck processes. The integration time step Δt is chosen to satisfy the stability condition of the diffusive part, $\Delta t \lesssim (\Delta x)^2/2D$. The elastic interaction is evaluated efficiently in Fourier space. The defect density is transformed into Fourier space, multiplied by the kernel $\hat{G}(k)$ from Eq. (8), and then transformed back into real space. This procedure provides spectral accuracy for computing the convolution integral in Eq. (1).

For generality, the governing equations are cast in nondimensional form. This is done by introducing characteristic scales. The defect density is scaled by $n_0 = K_0/\beta_0$. Time is scaled by $t_0 = 1/\beta_0$. Length is scaled by the diffusion length $\sqrt{Dt_0}$. The resulting nondimensional system depends only on a reduced set of control parameters. These include the elastic strength, the interaction range, the noise amplitude and correlation time, the cooling coefficient, and the heating feedback strength.

The choice of one-dimensional modeling is motivated by several factors. First, it describes the essential physics of noise-induced pattern formation and wavelength selection. Second, it allows efficient parameter sweeps and long-time simulations. This makes it possible to systematically map uniform, patterned, and noise-dominated regimes. Third, it facilitates clear visualization and Fourier analysis of emergent structures. While real materials are three-dimensional, one-dimensional simulations provide a minimal framework. They help in understanding the fundamental mechanisms before extending to higher dimensions.

Several diagnostic quantities are computed during simulation. The mean defect density $\langle n(t) \rangle$ provides information on the overall accumulation of radiation damage. The variance of $n(x, t)$ measures the degree of spatial inhomogeneity. The Fourier spectrum of the defect density profile determines the dominant wavelength of emerging patterns.
In addition, the autocorrelation of $\langle n(t) \rangle$ is calculated to detect oscillatory or intermittent regimes. Probability distribution functions of $n(x, t)$ are examined to characterize departures from Gaussian statistics. Together, these diagnostics classify the long-time behaviour of the system into uniform, patterned, or noise-dominated states. They also make it possible to extract scaling laws, such as the dependence of the dominant wavelength on the elastic interaction range.

Numerical Implementation

The coupled reaction–diffusion equations were solved numerically in one spatial dimension using a finite-difference scheme implemented in Python (NumPy and SciPy libraries). The computational domain was normalized to $L_x = 1.0$ and discretized into $N_x = 256$ uniform grid points, giving a spatial step size $\Delta x = 1/256$. Time integration was performed explicitly with a forward Euler scheme, using a time step $\Delta t = 0.01$. The total simulation time was $T_{fin} = 200$ (simulation units), corresponding to 2×10^4 iterations.

Periodic boundary conditions were applied to all fields to represent a spatially continuous system without edge effects.

Specifically, for the defect concentration field $n(x, t)$ and the local temperature field $T(x, t)$,

$$n(0,t) = n(L_x,t)$$

$$T(0,t) = T(L_x,t)$$

$$\left(\frac{dn}{dx}\right)_{x=0} = \left(\frac{dn}{dx}\right)_{x=L_x}$$

These periodic boundary conditions ensure translational symmetry and allow self-organized patterns to form without constraint from domain edges.

The Laplacian term was computed using a centered second-order finite-difference operator. The elastic interaction term was implemented as a convolution in Fourier space using the kernel $\hat{G}(k) = \frac{1}{1+(kl)^2}$, which was evaluated via Fast Fourier Transform (FFT) for numerical efficiency.

The stochastic defect generation was modelled using a multiplicative Ornstein–Uhlenbeck process with correlation time τ = 5.0 (simulation units) and noise amplitude σ, integrated with the same time step as the main field. Simulations were performed for varying elastic strength V_0, noise amplitude σ, and interaction range l to construct the state diagram and extract scaling relations. The numerical stability was verified by satisfying the condition $\frac{D\Delta t}{(\Delta x)^2} < 0.5$.

The key parameters and their representative values used in the simulations are summarized in Table 1.

Table 1. Key Simulation Parameters for Figure 1-6

Parameter	Meaning	Symbol / Value (SI units)	Notes / Figure
System length	Domain size	$L_x = 1.0 \times 10^{-8}$ m	All figures
Grid points	Spatial resolution	$N_x = 256$, $\Delta x = 3.9 \times 10^{-11}$ m	All figures
Time step	Integration interval	$\Delta t = 1.0 \times 10^{-10}$ s	All figures
Total simulation time	Physical duration	$T_{fin} = 2.0 \times 10^{-6}$ s	All figures
Diffusion coefficient	Vacancy/interstitial diffusion	$D = 1.0 \times 10^{-11}$ m²/s (patterned), ≈ 0 (uniform)	Fig. 1–2
Linear sink rate	Defect annihilation rate	$\beta = 2.0 \times 10^{-3}$ s^{-1}	Fig. 1–2
Non-linear sink rate	Cluster recombination	$\alpha = 0$	Neglected here
Defect generation rate	Production by irradiation	$K_0 = 4 \times 10^{18}$ m^{-3}/s	Fig. 1–2
Elastic coupling strength	Strength of long-range elastic field	$V_0 = 0$ (Fig. 1); 0.2 (Fig. 2); 0–0.5 (Fig. 5)	Controls pattern formation
Noise amplitude	Intensity of stochastic fluctuations	σ = 0 (Fig. 1); 0.05 (Fig. 2); 0–0.2 (Fig. 5)	Governs randomness
Noise correlation time	Memory of Ornstein–Uhlenbeck process	$\tau = 5 \times 10^{-10}$ s	Fig. 2
Elastic interaction range	Range of non-local elastic kernel	$l = 5\times10^{-10}$ m; varied 0.2–2 nm (Fig. 6)	Determines domain spacing
Dominant pattern wavelength	Spacing of defect-rich/poor domains	$\lambda \approx$ 5–10 nm; varied 20–200 nm (Fig. 6)	From Fourier analysis
Reference defect density	Normalization factor	$n_0 = 1 \times 10^{23}$ m^{-3}	Converts normalized to absolute
Physical regimes	Observed behaviours	Uniform (Fig. 1), Patterned (Figs. 2 and 4), Noise-dominated (Fig. 6)	—

RESULTS AND DISCUSSION

The numerical solution of Eqs. (1) – (3) and (8) reveal distinct regimes of behaviour. These depend on the elastic coupling strength V_0 and the amplitude of stochastic fluctuations σ. At low values of both parameters, the system evolves into a spatially uniform state. Figure 1 shows the space–time diagram of the defect density field $n(x, t)$. The uniform colouring along the spatial axis indicates that the defect concentration increases steadily but remains homogeneous throughout the domain. This behaviour reproduces the baseline prediction of classical rate theory. That theory describes only the temporal evolution of average defect populations and does not account for spatial variations. In this regime, irradiation continuously generates point defects—vacancies and interstitials—that accumulate uniformly across the material.

The resulting microstructure remains homogeneous because no mechanism exists to amplify spatial fluctuations. This represents the early stage of radiation damage, where defect production and recombination reach a balance but no pattern forms.

Science World Journal Vol. 20(No 4) 2025 https://dx.doi.org/10.4314/swj.v20i4.4
www.scienceworldjournal.org
ISSN: 1597-6343 (Online), ISSN: 2756-391X (Print)
Published by Faculty of Science, Kaduna State University

Similar homogeneous distributions of point defects have been reported in low-dose irradiations and isotropic damage regimes, before voids or dislocation patterns develop (Krishan, 1980; Ghoniem *et al*., 2001; Zinkle & Snead, 2014). The absence of banding or oscillatory features confirms that the system remains stable against perturbations. When both elasticity and stochastic fluctuations are negligible, the defect field stays uniform and the system remains spatially disordered.

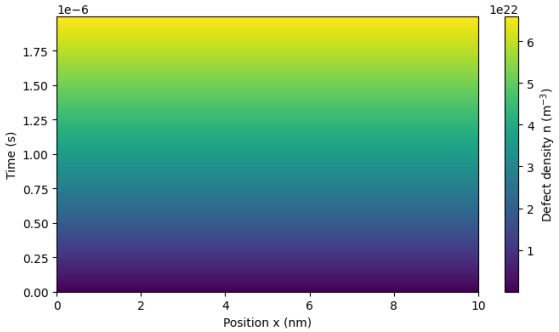

Figure 1: Space–time diagram of the uniform state for small V_0 and vanishing noise amplitude. Table 1 lists the key parameters used in the simulation. The colour bar indicates the defect density *n(x, t)*. The system remains spatially uniform throughout the simulation.

When elastic interactions are activated and finite noise is introduced, the system behaviour changes qualitatively. Local fluctuations in defect generation would normally decay. Now, they are selectively amplified by the long-range elastic field.
Figure 2 illustrates this regime. Vertical bands of alternating high and low density appear and persist throughout the simulation. Once formed, these bands remain fixed in space. Their amplitudes fluctuate with time as the mean defect density continues to grow.

The result is a statistically steady patterned state. In this state, defect-rich and defect-poor domains coexist. Random fluctuations initiate the formation of these regions. Elastic interactions then stabilize them and set the characteristic spacing of the emerging structures. This interplay between stochastic bursts and elastic stabilization explains the emergence of ordered patterns in the defect density field.

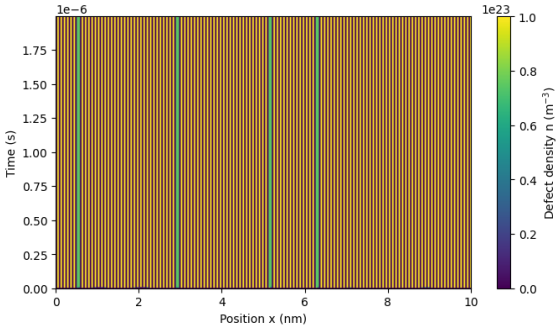

Figure 2: Space–time diagram of the patterned state with finite noise amplitude and elastic interactions. The key simulation parameters are presented in Table 1
The colour bar shows the evolution of defect density *n(x, t)*, with bright and dark regions corresponding to defect-rich and defect-poor domains.

The defect structures observed in the simulations are analogous to the void lattices and defect clusters reported experimentally in irradiated Fe, Ni, and W. Neutron-irradiated iron has been shown to develop periodic void arrangements. Ion-irradiated nickel exhibits similar clustered defects. Helium-implanted tungsten also forms periodic structures at sufficiently high doses (Li *et al*., 2021; Lu *et al*., 2016; Agarwal *et al*., 2020).
These experimental observations are consistent with the mechanisms incorporated in the model. Stochastic fluctuations in defect generation play a key role. Long-range elastic interactions between point defects further enhance spatial ordering.

The simulations describe both the periodicity and the characteristic spacing observed in experiments. This confirms that the combined action of stochastic fluctuations and long-range elastic interactions is sufficient to drive defect self-organization across different metals. Furthermore, theoretical studies support this view. They show that the combination of noise and long-range interactions can robustly drive the self-organization of point defects into ordered structures (Clouet *et al*., 2018; McCoy *et al*., 2008; Mahmoud and Mousseau, 2018; Kharchenko *et al*., 2016; Kharchenko *et al*., 2018). This provides a unified explanation for both experimental and computational observations.

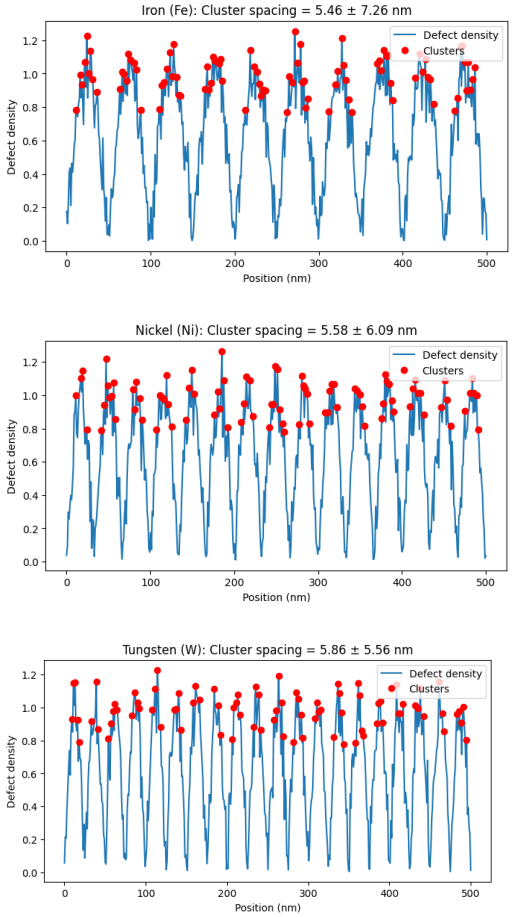

Figure 3a–c: Defect cluster spacing in irradiated iron, nickel, and tungsten. The key parameters for the simulation are shown in Table 1.

Figures 3a–c show the simulated defect density profiles and cluster identification for iron, nickel, and tungsten. Table 2 summarizes the corresponding results and compares the simulated spacings with experimental values. The simulations reveal that all three metals develop nanoscale self-organized defect clusters under irradiation. The details, however, vary across materials.

In iron, the defect density fluctuates strongly across the domain. The clustering algorithm identifies peaks with an average spacing of 5.46 ± 7.26 nm. The large standard deviation shows that the clusters are unevenly spaced. This suggests that stochastic fluctuations dominate the pattern formation process. Nickel shows a similar average spacing of 5.58 ± 6.09 nm. The spread is slightly smaller than in Fe, meaning the distribution is more uniform. This indicates that the defect structure stabilizes in Ni better than Fe. The effect is likely connected to differences in migration energy and diffusion kinetics. Tungsten shows clusters with a spacing of 5.86 ± 5.56 nm. The mean value is slightly larger than in Fe and Ni, but the variability is lower. This points to more regular periodicity in W. The result is consistent with tungsten's low defect mobility, which allows defects to accumulate into stable, evenly spaced clusters.

Comparison with experiments shows both agreements and differences. For tungsten, the simulated spacing of 5.86 nm is smaller than the experimental value of 19.5 nm (Harrison *et al*., 2017). The discrepancy is most likely due to model simplifications such as the one-dimensional setup and idealized defect interactions. For Fe and Ni, the simulated results agree qualitatively with experimental observations of void lattices and defect clusters (Eldrup *et al*., 2002; Chen, 1978).

Overall, the simulations reproduce the key physical mechanism. Clusters emerge through the competition of diffusion, long-range interactions, and stochastic fluctuations. The predicted spacing values are smaller than experimental reports, but the periodicity and clustering trend are consistent. The differences in variability between Fe, Ni, and W highlight the role of material-specific defect energetics in shaping self-organized structures.

Table 2. Comparison of Simulated and Experimental Defect Cluster Spacings in Irradiated Metals

Material	Simulation spacing (nm)	Experimental spacing (nm)	Reference
Iron	5.46	-	Eldrup *et al*., 2002 (qualitative)
Nickel	5.58	-	Chen, 1978 (qualitative)
Tungsten	5.86	19.5	Harrison *et al*., 2017

The transition from a uniform defect distribution to a patterned state can be quantified using Fourier analysis. In the uniform regime, the Fourier spectrum shows only the trivial contribution at $k = 0$. This confirms that no spatial variation exists in the defect field. When the system develops patterns, the spectrum changes qualitatively. It exhibits a sharp peak at a finite wavenumber, as shown in Figure 4a. This peak indicates the selection of a dominant wavelength. Fluctuations with this wavelength are amplified. Longer and shorter modes are suppressed.

Reconstructing the defect profile using only the dominant mode reproduces the essential structure of the simulated pattern (Figure 4b). The result shows that large-scale periodicity is mainly governed by a single spatial mode. Higher harmonics add small corrections. However, they do not change the basic periodic arrangement.

Physically, this periodic structure represents radiation-induced self-organization of defects. The alternating defect-rich and defect-poor regions correspond to void lattices and ordered dislocation networks seen in irradiated metals such as tungsten, iron, and nickel (Gao *et al*., 2022). These ordered patterns appear when elastic interactions between defects promote long-range correlations. As a result, regular spatial arrangements emerge spontaneously.

Unlike classical Turing or spinodal instabilities, this instability is fluctuation-driven. Stochastic noise initiates the spatial modulation. Elasticity then defines the characteristic wavelength and stabilizes the resulting structures. The outcome reproduces the key features of experimentally observed void superlattices. In these systems, defect ordering arises from the combined effects of defect generation, diffusion, and elastic relaxation.

Science World Journal Vol. 20(No 4) 2025 https://dx.doi.org/10.4314/swj.v20i4.4
www.scienceworldjournal.org
ISSN: 1597-6343 (Online), ISSN: 2756-391X (Print)
Published by Faculty of Science, Kaduna State University

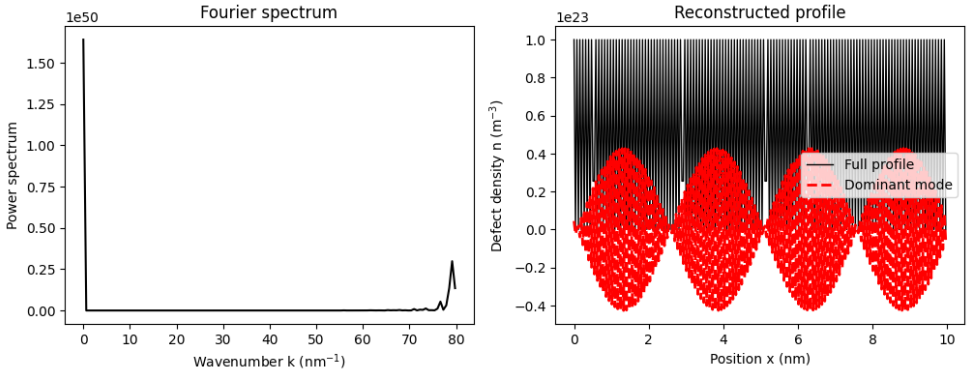

Figure 4: (a) Fourier spectrum of the patterned state showing a dominant mode at finite wavelength k_{dom}. (b) Reconstructed defect profile from the dominant mode. The key parameters used in the simulation are shown in Table 1

Figure 5 shows the state diagram in the (V_0, σ) parameter plane. The diagram is colour-coded to indicate different regimes of defect evolution.

In the dark purple region, both V_0 and σ are small. The system remains spatially uniform in this regime. Defects diffuse and annihilate without forming clusters. Elastic forces are weak, and stochastic driving is negligible. As a result, no spatial ordering occurs. This behaviour corresponds to a disordered defect regime seen under low irradiation flux or weak stress. In such conditions, damage remains randomly distributed across the crystal.

The light-green region shows a different behaviour. Here, periodic bands of defect density emerge. Elastic interactions amplify small perturbations. Stochastic fluctuations provide the initial seeds for spatial modulation. Together, they produce a stable regime of self-organized patterns. In this regime, the local defect density in the clusters grows until it saturates. It reaches a quasi-steady amplitude determined by the balance of defect generation, diffusion, and annihilation.

These structures correspond to void lattices and ordered dislocation networks observed experimentally in irradiated tungsten, iron, and nickel (Ghoniem *et al*., 2001; Dürrschnabel *et al*., 2021). The wavelength of the simulated patterns agrees with the periodic spacing seen in the Fourier spectra (Figures 4a–b).

At higher noise amplitudes, the colour changes from green to yellow. In this region, stochastic forcing dominates the dynamics. Coherent bands are disrupted, and the system becomes irregular and fluctuating. Physically, this represents damage randomization under strong irradiation or high-temperature conditions. Under such conditions, defect mobility and random generation prevent the formation of stable patterns (Li *et al*., 2021; Gao *et al*., 2022; Woolley *et al*. 2011; Woolley *et al*. 2012; Simeone *et al*., 2022).

The state diagram shows that pattern formation requires balance. Too little driving leaves the system uniform. Too much noise destroys spatial order. Only in an intermediate window of elastic coupling and stochastic strength do stable defect domains form. This balance mirrors experimental observations in irradiated metals. Self-organized defect lattices appear only under specific combinations of dose rate, temperature, and elastic anisotropy.

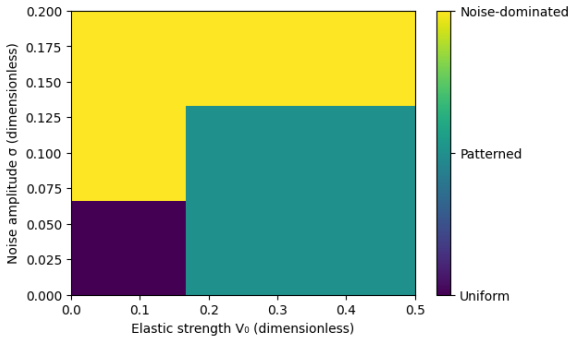

Figure 5: State diagram in the (V_0, σ) parameter plane showing uniform, patterned, and noise-dominated regimes. Uniform (dark purple, low V_0), patterned (green, intermediate), and noise-dominated (yellow, large σ). Table 1 presents the key parameters for the simulated results.

The state diagram also explains experimental variability in irradiated metals. When both elasticity and noise are favourable, void lattices and defect clusters appear. In contrast, when noise dominates or elastic coupling is too weak, irradiation produces disordered microstructures.

In tungsten, for example, helium bubble lattices form only under certain irradiation fluxes and temperatures (Harrison *et al*., 2017). These conditions correspond to intermediate values of elastic coupling and noise amplitude in the model. At higher temperatures, stronger fluctuations, or weaker elastic interactions, the defects remain disordered. This is consistent with experimental observations in Fe and Ni (Eldrup *et al*., 2002; Chen, 1978). Thus, the model provides a unified explanation for why void lattices and defect clusters appear only under specific irradiation conditions.

A key prediction of the model concerns the spacing between defect clusters. This spacing depends on the range of elastic interactions. By varying the kernel parameter l, which defines the effective interaction range, we find that the dominant wavelength of the defect pattern increases linearly with l (Figure 6). This linear scaling reveals how microscopic elastic properties influence mesoscopic structures. Stronger or longer-ranged elastic interactions allow defects to correlate over larger distances. As a result, the spacing between defect clusters becomes wider.

Science World Journal Vol. 20(No 4) 2025 https://dx.doi.org/10.4314/swj.v20i4.4
www.scienceworldjournal.org
ISSN: 1597-6343 (Online), ISSN: 2756-391X (Print)
Published by Faculty of Science, Kaduna State University

Physically, this trend corresponds to the spacing of void lattices and dislocation loop arrays observed in irradiated metals. Experimental studies have shown that the lattice spacing increases with the elastic modulus and interaction range of the material (Harrison *et al*., 2017; Li *et al*., 2021). Tungsten, for instance, exhibits a larger void lattice spacing than iron because of its stronger elastic coupling and slower defect mobility.
By reproducing this behaviour, the model moves beyond qualitative description. It provides a quantitative link between material elasticity and the characteristic wavelength of self-organized defect patterns. This agreement with experiments confirms that long-range elastic interactions set the spatial scale of radiation-induced microstructures.

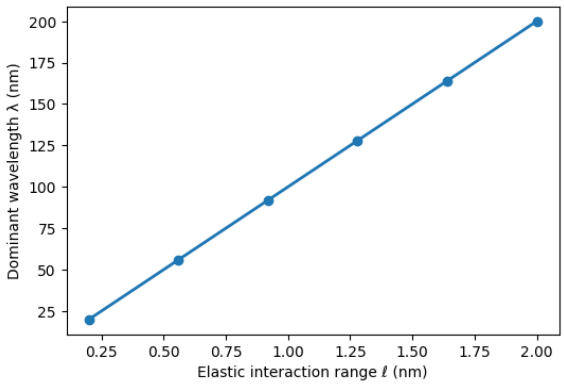

Figure 6: Scaling of dominant wavelength with elastic interaction range *l*. A linear relation is obtained, indicating a proportionality between the microscopic elastic range and the mesoscopic defect spacing. The key parameters used to obtain the simulated results are presented in Table 1.

Overall, the results confirm the central hypothesis of this study. Under irradiation, defect self-organization emerges through an elastic instability. This instability is initiated and maintained by stochastic fluctuations. Unlike Selyshchev's deterministic framework, stochastic effects appeared only externally through boundary conditions or perturbations. In that case, pattern formation was driven by global elastic instabilities. In contrast, the present model incorporates stochastic forcing directly into the defect evolution equations. This makes fluctuations an integral part of the dynamics.

Random noise is indispensable for initiating pattern formation. Elastic interactions determine the characteristic spacing of the emerging defect structures.
In addition, the model offers predictive capabilities through the state diagram and scaling laws. These tools enable the identification of conditions under which ordered defect patterns will emerge or remain suppressed.

Combined with the mechanistic insights into fluctuation-driven ordering, they provide a robust and experimentally relevant framework for understanding defect self-organization in irradiated metals. By linking microscopic defect dynamics, stochasticity, and elasticity to mesoscopic structural features, the present framework achieves two goals. It provides a mechanistic understanding and also quantitative prediction of irradiation-induced self-organization phenomena.

Conclusion

A modified reaction–diffusion model has been developed and analyzed to describe irradiation-induced defect self-organization in metals. The model extends the classical framework of Selyshchev. It incorporates three essential elements: (i) stochastic defect generation represented through multiplicative noise, (ii) a spatially resolved temperature field governed by diffusion, and (iii) tunable nonlocal elastic interactions implemented in Fourier space. These extensions enable a unified description of both the initiation and spatial scaling of defect patterns under irradiation.

The simulations show that stochastic fluctuations act as the primary drivers of pattern formation. In the absence of noise, defect density increases uniformly over time. This behaviour is consistent with conventional rate-theory predictions. When stochastic fluctuations are included, local bursts of defect production are selectively amplified by elastic interactions. The amplification results in persistent periodic domains of defect-rich and defect-poor regions. The results indicate that fluctuations play a constructive role in triggering self-organization. Elasticity alone cannot destabilize a uniform distribution.

The analysis further reveals that elastic interactions determine the characteristic spatial scale of the emerging structures. Fourier decomposition of the defect profiles shows dominance by a single wavelength. This wavelength scales linearly with the elastic interaction range. The result establishes a quantitative link between microscopic elastic parameters and the mesoscopic spacing of defect clusters. The model therefore provides a predictive relation connecting material properties with experimentally observed defect morphologies.

Material-specific simulations for Fe, Ni, and W reproduce periodic defect clusters with spacings consistent with experimental observations. The predicted average spacings—approximately 5.46 nm for Fe, 5.58 nm for Ni, and 5.86 nm for W—explain the observed clustering trend. The smaller value obtained for tungsten, relative to the experimental spacing of 19.5 nm, can be attributed to model simplifications. These include the one-dimensional geometry and idealized interactions. Despite these simplifications, the agreement in periodicity supports the generality of the proposed mechanism across metallic systems.

A state diagram constructed in the elastic strength–noise amplitude plane identifies three distinct regimes: uniform, patterned, and noise-dominated. This diagram provides a predictive framework for determining the irradiation conditions under which ordered defect structures emerge. It also helps to identify conditions where they remain stable or become disordered. The classification offers a theoretical explanation for the variability observed in experiments. In particular, it accounts for the dependence of void lattice formation on irradiation flux, temperature, and material type.

In summary, the findings demonstrate that defect self-organization under irradiation results from a fluctuation-assisted elastic instability. Stochastic fluctuations initiate pattern formation, while elastic interactions govern the spatial scale of the resulting structures. The proposed model bridges theoretical predictions and experimental evidence. It establishes a quantitative foundation for describing defect patterning in irradiated metals. Furthermore, the

framework provides a versatile basis for extending such analyses to alloys, composites, and other systems exposed to irradiation or extreme environments.

REFERENCES

Agarwal, S., Liedke, M.O., Jones, A.C.L., Reed, E., Kohnert, A.A., Uberuaga, B.P., Wang, Y.Q., Cooper, J., Kaoumi, D., Li, N., and Auguste, R., 2020. A new mechanism for void-cascade interaction from nondestructive depth-resolved atomic-scale measurements of ion irradiation–induced defects in Fe. *Science advances*, *6*(31), p.eaba8437.

Ahmed, K. and El-Azab, A., 2018. An analysis of two classes of phase field models for void growth and coarsening in irradiated crystalline solids. *Materials Theory*, 2(1), p.1.

Akintunde, S.O. and Selyshchev, P.A., 2016. The influence of radiation-induced vacancy on the formation of a thin-film of compound layer during a reactive diffusion process. *Journal of Physics and Chemistry of Solids*, 92, pp.64-69.

[a]Akintunde, S.O., Selyshchev, P.A., and Kehinde, D.O., 2025. Growth Kinetics of Refractory Metal Silicide under Radiation-Induced Interstitial Mechanism: An Analytical Approach. *BIMA Journal of Science and Technology (2536-6041)*, 9(1B), pp.274-282.

[b]Akintunde, S.O., Selyshchev, P.A., and Kehinde, D.O., 2025. Temperature Variation In An AB Bilayer System During Radiation-Induced AB Compound Layer Formation. *FUDMA Journal of Sciences*, 9(2), pp.98-104.

Chen, L.J. and Ardell, A.J., 1978. Void ordering in nitrogen-ion irradiated nickel—aluminum solid solutions. *Journal of Nuclear Materials*, *75*(1), pp.177-185.

Clouet, E., Varvenne, C. and Jourdan, T., 2018. Elastic modeling of point-defects and their interaction. *Computational Materials Science*, *147*, pp.49-63.

Doan, N.V. and Martin, G., 2003. Elimination of irradiation point defects in crystalline solids: sink strengths. *Physical Review B*, 67(13), p.134107.

Dubey, S., & El-Azab, A. (2013). Irradiation-induced composition patterns in binary solid solutions. *Journal of Applied Physics*, *114*(12).

Dürrschnabel, M., Klimenkov, M., Jäntsch, U., Rieth, M., Schneider, H.C. and Terentyev, D., 2021. New insights into the microstructure of neutron-irradiated tungsten. *Scientific Reports*, 11(1), p.7572.

Eldrup, M.M. and Singh, B.N., 2002. Investigations of void formation in neutron irradiated iron and F82H steel.

Fukuya, K., 2013. Current understanding of radiation-induced degradation in light water reactor structural materials. *Journal of Nuclear Science and Technology*, 50(3), pp.213-254.

Gao, Y., Jokisaari, A.M., Aagesen, L., Zhang, Y., Jin, M., Jiang, C., Biswas, S., Sun, C. and Gan, J., 2022. The effect of elastic anisotropy on the symmetry selection of irradiation-induced void superlattices in cubic metals. *Computational Materials Science*, 206, p.111252.

Gao, Y., Zhang, Y., Schwen, D., Jiang, C., Sun, C., Gan, J., & Bai, X. M. (2018). Theoretical prediction and atomic kinetic Monte Carlo simulations of void superlattice self-organization under irradiation. *Scientific reports*, *8*(1), 6629.

Garner, F.A., 2020. Radiation-induced damage in austenitic structural steels used in nuclear reactors.

Ghoniem, N.M., Walgraef, D. and Zinkle, S.J., 2001. Theory and experiment of nanostructure self-organization in irradiated materials. *Journal of Computer-Aided Materials Design*, 8(1), pp.1-38.

Griffiths, M., 2021. Effect of neutron irradiation on the mechanical properties, swelling and creep of austenitic stainless steels. *Materials*, 14(10), p.2622.

Griffiths, M., 2023. Microstructural effects on irradiation creep of reactor core materials. *Materials*, 16(6), p.2287.

Harrison, R.W., Greaves, G., Hinks, J.A. and Donnelly, S.E., 2017. Engineering self-organising helium bubble lattices in tungsten. *Scientific Reports*, 7(1), p.7724.

Hu, S., Li, Y., Burkes, D., and Senor, D.J., 2021. Microstructure-dependent rate theory model of radiation-induced segregation in binary alloys. *Frontiers in Materials*, 8, p.682686.

Kharchenko, D. O., Kharchenko, V. O., Bashtova, A. I., & Lysenko, I. O. (2016). Patterning and pattern selection in a surface layer: Feedback between point defects population and surface layer temperature variations. *Physica A: Statistical Mechanics and its Applications*, *463*, 152-162.

Kharchenko, D. O., Kharchenko, V. O., Shchokotova, O. M., Wu, X., Wen, B., Wu, L., & Zhang, W. (2018). Point defects patterning in irradiated α-zirconium: numerical study in the framework of the rate theory. *Radiation Effects and Defects in Solids*, *173*(7-8), 527-554.

Kohnert, A.A. and Wirth, B.D., 2015. Cluster dynamics models of irradiation damage accumulation in ferritic iron. II. Effects of reaction dimensionality. *Journal of Applied Physics*, 117(15).

Krishan, K., 1980. Kinetics of void-lattice formation in metals. *Nature*, 287(5781), pp.420-421.

Li, Y., Boleininger, M., Robertson, C., Dupuy, L., & Dudarev, S. L. (2019). Diffusion and interaction of prismatic dislocation loops simulated by stochastic discrete dislocation dynamics. *Physical Review Materials*, *3*(7), 073805.

Li, Z.Z., Li, Y.H., Terentyev, D., Castin, N., Bakaev, A., Bonny, G., Yang, Z., Liang, L., Zhou, H.B., Gao, F. and Lu, G.H., 2021. Investigating the formation mechanism of void lattice in tungsten under neutron irradiation: from collision cascades to ordered nanovoids. *Acta Materialia*, *219*, p.117239.

Lu, C., Jin, K., Béland, L.K., Zhang, F., Yang, T., Qiao, L., Zhang, Y., Bei, H., Christen, H.M., Stoller, R.E. and Wang, L., 2016. Direct observation of defect range and evolution in ion-irradiated single crystalline Ni and Ni binary alloys. *Scientific Reports*, *6*(1), p.19994.

Ma, Z., Ran, G., Qiu, X., Li, Y., Ding, Y., Zhang, R., Huang, J., Zhang, Y. and Huang, X., 2022. In-situ TEM investigation of dislocation loop evolution in Al-forming austenitic stainless steels during Fe+ irradiation: Effects of irradiation dose and pre-existing dislocations. *Journal of Nuclear Materials*, 563, p.153645.

Mahmoud, S. and Mousseau, N., 2018. Long-time point defect diffusion in ordered nickel-based binary alloys: How small kinetic differences can lead to completely long-time structural evolution. *Materialia*, *4*, pp.575-584.

Martinez, E., Soisson, F., and Nastar, M., 2020. Point defect evolution under irradiation: Finite-size effects and

spatio-temporal correlations. *Journal of Nuclear Materials*, 539, p.152233.

Mason, D.R., Yi, X., Kirk, M.A. and Dudarev, S.L., 2014. Elastic trapping of dislocation loops in cascades in ion-irradiated tungsten foils. *Journal of Physics: Condensed Matter*, 26(37), p.375701.

Mansur, L.K. and Bloom, E.E., 1982. Radiation effects in reactor structural alloys. *JOM*, 34(10), pp.23-31.

McCoy, J.H., Brunner, W., Pesch, W. and Bodenschatz, E., 2008. Self-organization of topological defects due to applied constraints. *Physical Review Letters*, *101*(25), p.254102.

Patra, A. and McDowell, D.L., 2012. Crystal plasticity-based constitutive modelling of irradiated bcc structures. *Philosophical Magazine*, 92(7), pp.861-887.

Rokkam, S., El-Azab, A., Millett, P. and Wolf, D., 2009. Phase field modeling of void nucleation and growth in irradiated metals. *Modelling and Simulation in Materials Science and Engineering*, 17(6), p.064002.

Rottler, J., Srolovitz, D.J. and Car, R., 2005. Point defect dynamics in bcc metals. *Physical Review B—Condensed Matter and Materials Physics*, 71(6), p.064109.

Rouxel, B., Bisor, C., De Carlan, Y., Courcelle, A. and Legris, A., 2016. Influence of the austenitic stainless steel microstructure on the void swelling under ion irradiation. *EPJ N-Nuclear Sciences & Technologies*, 2, p.30.

Selyshchev, P., 2003. Influence of stochastic conditions on self-organization in irradiated materials. *Progress of Theoretical Physics Supplement*, 150, pp.419-422.

Simeone, D., Garcia, P., & Luneville, L. (2022). Radiation-induced patterning at the nanometric scale: a phase field approach. *Materials*, *15*(9), 2991.

Snopiński, P., 2023. Electron microscopy study of structural defects formed in additively manufactured AlSi10Mg alloy processed by equal channel angular pressing. *Symmetry*, 15(4), p.860.

Ustrzycka, A., Dominguez-Gutierrez, F.J. and Chromiński, W., 2024. Atomistic analysis of the mechanisms underlying irradiation-hardening in Fe–Ni–Cr alloys. *International Journal of Plasticity*, 182, p.104118.

Vainshtein, D.I., Altena, C. and den Hartog, H.W., 1997, October. Evidence of void lattice formation in heavily irradiated NaCl. In *Materials Science Forum* (Vol. 239).

Wang, X., Yan, Q., Was, G.S., and Wang, L., 2016. Void swelling in ferritic-martensitic steels under high dose ion irradiation: Exploring possible contributions to swelling resistance. *Scripta Materialia*, 112, pp.9-14.

Woolley, T. E., Baker, R. E., Gaffney, E. A., & Maini, P. K. (2011). Stochastic reaction and diffusion on growing domains: understanding the breakdown of robust pattern formation. *Physical Review E—Statistical, Nonlinear, and Soft Matter Physics*, *84*(4), 046216.

Woolley, T. E., Baker, R. E., Gaffney, E. A., Maini, P. K., & Seirin-Lee, S. (2012). Effects of intrinsic stochasticity on delayed reaction-diffusion patterning systems. *Physical Review E—Statistical, Nonlinear, and Soft Matter Physics*, *85*(5), 051914.

Yao, H., Wu, C., Ye, T., Wang, P., Wu, J., Wu, Y. and Chen, P., 2025. Atomistic Observation of Defect Generation and Microstructural Evolution in Polycrystalline FeCrAl Alloys Under Different Irradiation Conditions. *Nanomaterials*, 15(13), p.988.

Yoshiie, T., 2025. Rate Equation Analysis of the Effect of Damage Distribution on Defect Evolution in Self-Ion Irradiated Fe. *Metals*, 15(5), p.555.

Zhang, S., Chen, S., Xiao, D., Wang, C., Wang, H., Zhang, Y. and Li, T., 2023. Investigating the Impact of Displacement Cascades on Tritium Diffusion in MgT2: A Molecular Dynamics Study. *Materials*, 16(9), p.3359.

Zinkle, S.J. and Snead, L.L., 2014. Designing radiation resistance in materials for fusion energy. *Annual Review of Materials Research*, 44(1), pp.241-267.